15R.4 **CLIMATOLOGICAL ANALYSIS OF DSDs IN OKLAHOMA AS REVEALED BY 2D-VIDEO DISDROMETER AND POLARIMETRIC WSR-88D**

Terry J. Schuur, Alexander V. Ryzhkov, and Darren R. Clabo

Cooperative Institute for Mesoscale Meteorological Studies, The University of Oklahoma
and NOAA/OAR National Severe Storms Laboratory, Norman, Oklahoma

1. Introduction

Since the Spring of 1998, over 47,000 one-minute drop size distribution (DSD) measurements have been made by the National Severe Storms Laboratory 2D-video disdrometer (Schuur et al., 2001) in Norman, OK. Collected over many seasons and precipitation regimes, these DSDs reveal much information about natural DSD variability over the southern Great Plains. In this study, we use this large dataset to examine the relationship of the measured DSDs to season, a variety of storm and precipitation system types, continental and tropical precipitation, warm and cold season precipitation, surface temperature, and the height of the bright band. Measured DSDs are used to compute average dependencies of differential reflectivity (Z_{DR}) and specific differential phase (K_{DP}) on radar reflectivity (Z) for different storm types. Special consideration is given to the relative frequency and importance of DSDs dominated by big drops, characterized by an unusually large median volume diameter (D_0), and their impact on polarimetric rainfall estimation.

2. Data analysis

The 47,000 one-minute DSD measurements that constitute the dataset (all winter precipitation events that were known to contain snow images and all DSDs with rain rates below 0.1 mm h^{-1} were removed prior to analysis) were made on 273 separate days over an approximate 7 year period from April 20, 1998 through May 13, 2005. While the disdrometer did not run continuously over this 7 year period, the comprehensive dataset contains multiple events over a wide variety of seasons and precipitation regimes and accounts for 2.78 m of accumulated rainfall, which represents more than 3 times the average annual rainfall for central Oklahoma. Plots of rain rate versus time for each event in this dataset are at http://cimms.ou.edu/~schuur/disdcase/case.html.

Corresponding author address: Terry J. Schuur, National Severe Storms Laboratory
1313 Halley Circle, Norman, OK, 73069
email: Terry.Schuur@noaa.gov

As noted, the goal of this study is to examine the relationship of observed DSDs to a variety of potential seasonal dependencies, precipitation types, and environmental conditions. To accomplish this, a searchable data base was created. Season and month of occurrence, the height of the 0°C and 5°C isotherms (obtained from sounding data), and surface data (obtained from the nearby Oklahoma mesonet site) were input for each one-minute DSD. In order to classify the DSDs by storm type, radar data from the operational KTLX WSR-88D radar, located in central Oklahoma, were obtained from the National Climatic Data Center for all precipitation events with at least 1 mm of accumulated rainfall, accounting for 222 events and 95 % of the total DSDs. Base scan images for each volume were then generated, looped, and compared against rain rate versus time plots for each event. Based on this analysis, all DSDs were classified into the following broad precipitation categories: Synoptic, Mesoscale Convective System, Isolated Storms and Showers, and Supercell. For the Synoptic and Mesoscale Convective System categories, the precipitation was further categorized into transition zone (MCS only), stratiform, and embedded convection categories. A Hail category was created to include all storms in which hail was known to have been collected by the disdrometer. Finally, an analysis of sounding and DSD data for each event was used to create a Tropical category. The combined database allowed DSDs to be easily extracted an analyzed for a wide combination of precipitation types and environmental conditions.

All DSDs were processed to compute the polarimetric variables of Z, Z_{DR}, and K_{DP} using the assumed drop aspect ratio of Brandes et al. (2002, 2005). Due to the large number (nearly 30 million) of drops detected, it was not possible to identify each hail stone in the dataset. As a result, some DSDs may contain images that were erroneously assumed, for the purpose of polarimetric calculations, to be large drops, thereby leading to a higher Z_{DR} than would be expected if sampled by radar, particularly at reflectivities > 50 dBZ. As much as possible, however, records were taken on which precipitation systems contained hail over the entire data collection period; all 10 events that

were recorded to have contained hail have been grouped accordingly. We therefore believe that the influence of hail on Z_{DR} and K_{DP} computations for most precipitation categories presented here is quite minimal. In this study, we primarily use Z-Z_{DR} and Z-K_{DP} scatterplots to compare and contrast the various precipitation regimes. For most comparisons, Z_{DR} and K_{DP} are further averaged over 5 dBZ reflectivity bins to produce average profiles for each of the categories. While gamma functional fit parameters were also computed for all DSDs, they are not presented in this study and will be the subject of future analyses.

3. Seasonal variations

We first examine the relationship of DSDs to season. Fig. 1 presents a plot of Z-Z_{DR} (Z_{DR} averaged over 5 dBZ reflectivity bins) by month. Fig. 1 shows tremendous seasonal variation, especially for Z > 40 dBZ. In general, the spring months of March, April, and May (green lines) tend to have the largest Z_{DR} with respect to Z than any other season. This is probably due to the greater likelihood of rain drops containing small ice cores reaching the ground during the spring months. The Summer months of June, July, and August appear to fall in the middle of the spectrum with the smallest Z_{DR} with respect to Z occurring in the early Fall months of September and October. While the apparent transition to DSDs with smaller relative drops in the late Summer and into the early Fall is not at first obvious, it is probably related to the lower frequency of strong convection and somewhat higher freezing level in the late Summer (a discussion of the apparent relationship of freezing level to DSDs with smaller drops will follow in section 5). It should also be noted that many of the events categorized as Tropical, which are typically dominated by small drops, occurred during the early Fall.

Because all events in which snow was observed were removed from the analysis, very few DSDs with Z > 45 dBZ were observed during the Winter months. Non-frozen precipitation during this time of year tends to be light and fall from more widespread synoptic-scale systems. The most obvious outlier in Fig. 1 is the month of December. A closer examination of the data, however, reveals that the 92% of the rainfall in the December dataset fell during an unusually warm week in early December of 1999, during which several convective events that are quite uncharacteristic for that time of year passed over the disdrometer site. The dominance of this unusual month on the overall December dataset is illustrated well by Fig. 2, which shows surface temperatures computed by averaging over all

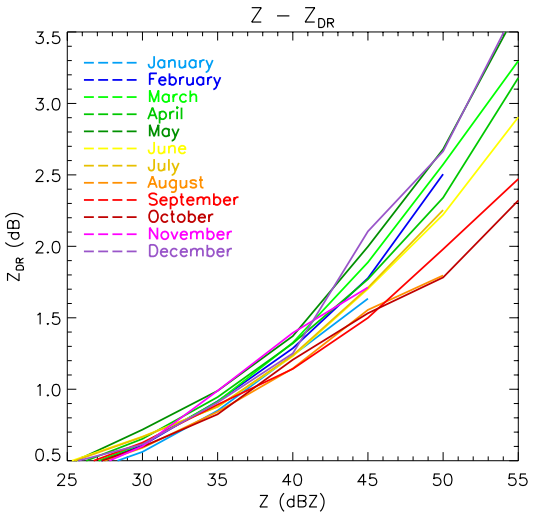

Fig. 1. Plot of Z-Z_{DR} by month of year. Z_{DR} has been averaged over 5 dBZ reflectivity bins.

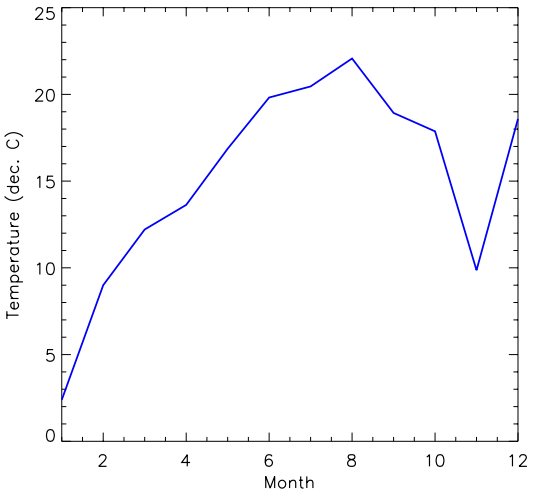

Fig. 2. Dataset average surface temperature by month of year. The average surface temperature was computed by averaging over all DSDs used in each month's analysis.

DSDs used in each month's analysis. Other than the unusually warm week in early December of 1999, which had an average surface temperature of more than 18ºC, it can be seen that the average temperature by month for this dataset follows a rather smooth annual profile that is similar to what one would expect from climatology.

4. DSD dependence on precipitation type

a. Comparison of precipitation systems

Using Z-Z_{DR} scatterplots obtained with the polarimetric KOUN WSR-88D radar, Ryzhkov et al. (2005) found that precipitation type can often

be categorized into specific regimes. In this section, we use DSD data examine the relationship between DSDs and precipitation type. A comparison of these precipitation types is shown by the Z-Z_{DR} plot (Z_{DR} averaged over 5 dBZ reflectivity bins) presented in Fig. 3. As noted earlier, precipitation was classified into Synoptic, Mesoscale Convective System, Isolated Showers and Storms, Hail, and Tropical categories. Hereafter, we refer to these categories as SYNOP, MCS, ISHOW, HAIL, and TROP, respectively. A Supercell category did not contain a sufficient number of data points for analysis. Significant differences between the precipitation regimes are immediately apparent. Most obvious is the rather large differences between the TROP and HAIL categories, even at reflectivities as low as 25 dBZ. As noted in section 2, due to the large number of images, it was not possible to separate and identify images belonging to hail. As a result, computed Z_{DR}s for the hail category are probably somewhat higher than would be expected if observed by radar, especially at higher reflectivities. Despite this, the difference between the HAIL and TROP categories (as well as their difference from the SYNOP, MCS, and ISHOW categories) is substantial.

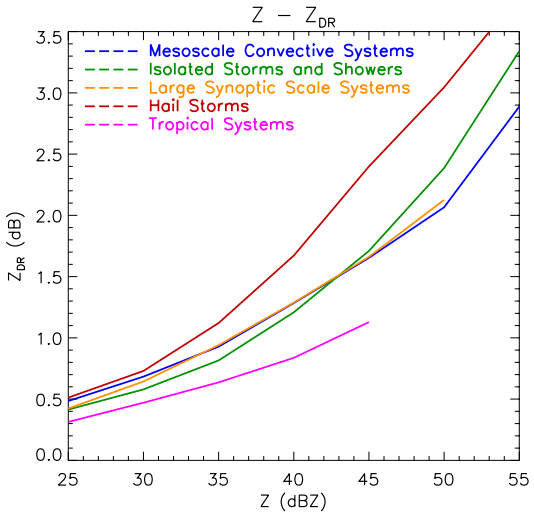

Fig. 3. Plot of Z-Z_{DR} by type of precipitation. Z_{DR} has been averaged over 5 dBZ reflectivity bins.

As would be expected, The SYNOP, MCS, and ISHOW categories fall in between TROP and HAIL. It is particularly interesting to note that the MCS and ISHOW profiles intersect at a location between 40 and 45 dBZ, with ISHOW having a lower average Z_{DR} at reflectivities less than approximately 42 dBZ and a higher average Z_{DR} at reflectivities greater than 42 dBZ. This is likely due to the significant influence of DSDs from stratiform precipitation in the MCS category where, at the lower reflectivities, the higher average MCS Z_{DR} can be attributed to the contribution from occasional big drops that form when large aggregates melt just below the freezing level. An absence of small drops due to evaporation in the stratiform region's unsaturated mesoscale downdraft (Brown, 1979) may also contribute to this difference. As would be expected, the SYNOP profile, which is typically due to widespread stratiform precipitation with little if any embedded convection, falls in between MCS and ISHOW.

b. Comparison of MCS stratiform to Synoptic stratiform precipitation

Given the large number of DSDs collected in stratiform precipitation and the influence of the stratiform DSDs on the overall statistics, we also explore the differences between MCS stratiform and SYNOP stratiform precipitation. Fig. 4 shows a Z-Z_{DR} and Z-K_{DP} scatterplot comparison of MCS stratiform (blue) and SYNOP stratiform (red) precipitation for all observed stratiform events. Fig. 5 summarizes Fig. 4 by presenting a Z-Z_{DR} comparison where Z_{DR} has been averaged over 5 dBZ reflectivity bins, showing that MCS stratiform precipitation has a higher Z_{DR}, with respect to Z, than SYNOP stratiform precipitation at all reflectivity levels. At 45 dBZ, the average MCS stratiform Z_{DR} is as much as 0.5 dB larger than the SYNOP Z_{DR}. In the case of an MCS, the stratiform region, at maturity, is the constant recipient of a steady influx of hydrometeors and positively buoyant air from the convective line. As a result, a strong mesoscale updraft that can add significant additional water mass through depositional growth to the detrained hydrometeors often develops, leading to large aggregates and a very intense radar bright band. This sort of convective contribution is generally absent in SYNOP events. Our observations suggest that peak reflectivities in MCS stratiform regions are typically much higher than in SYNOP stratiform regions. This is supported by the data presented in Fig. 5, which indicates that the drops that eventually form from the melting large aggregates result in larger drops and a correspondingly higher Z_{DR}s at the surface.

c. Comparison of MCS precipitation regimes

MCSs can sometimes represent a challenging rainfall estimation problem due to the dramatically different DSDs that often occur in their different precipitation regions. This is illustrated well by Fig. 6, which shows a Z-Z_{DR} and Z-K_{DP} scatterplot comparison of MCS convective (blue), transition zone (green), stratiform region (orange), and embedded convection (red) precipitation for all observed MCS events. Fig. 7 summarizes Fig. 6 by presenting Z-Z_{DR}, where Z_{DR} has been averaged over 5 dBZ reflectivity bins. It is interesting to

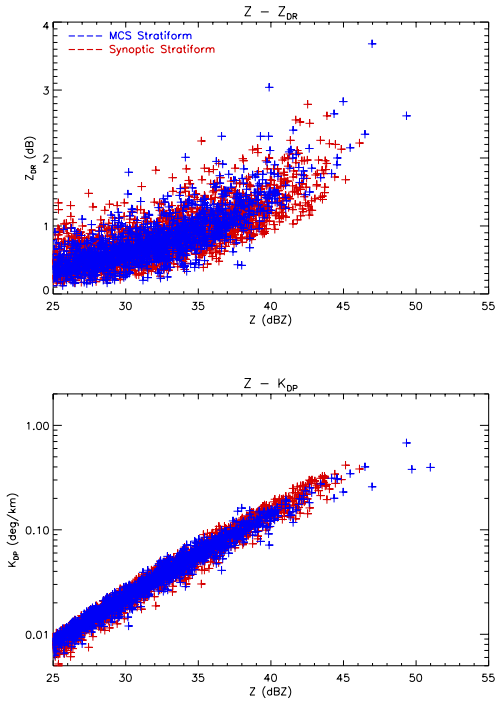

Fig. 4. Scatterplot of Z vs. Z_{DR} for Synoptic stratiform (red) and MCS stratiform (blue) precipitation.

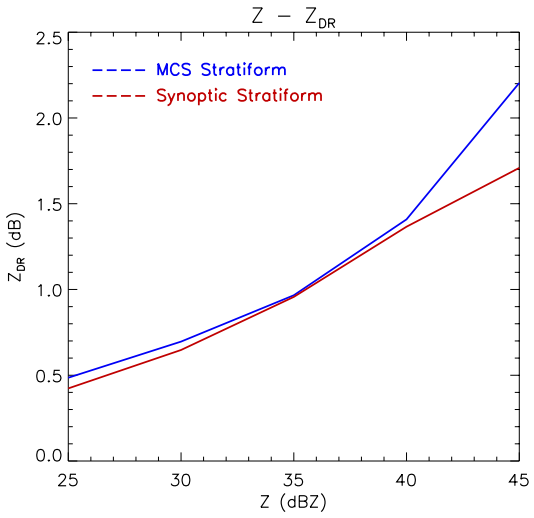

Fig. 5. Plot of Z-Z_{DR} for Synoptic and MCS stratiform precipitation. Z_{DR} has been averaged over 5 dBZ reflectivity bins.

note that the stratiform region has a higher average Z_{DR}, with respect to Z, than all of the other MCS precipitation regions, including the convective line. Our observations indicate that very high Z_{DR} measurements, associated with big drops forming in convective updrafts at the leading edge of the convective line, is a common feature in MCSs. The large number of DSDs collected in the convective line's intense precipitation region, which is a region of smaller, on average, drops and lower Z_{DR}, apparently masks the leading edge "big drop" region in the overall average. As would be expected, the transition zone, a region known for a deep downdraft and weak reflectivities, has the smallest average drop size.

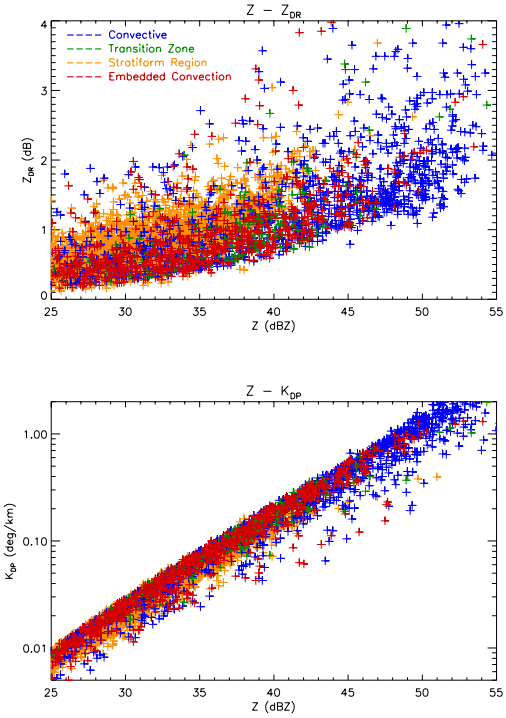

Fig. 6. Scatterplot of Z vs. Z_{DR} for convective (blue), transition zone (green), stratiform (orange), and embedded convection (red) MCS precipitation.

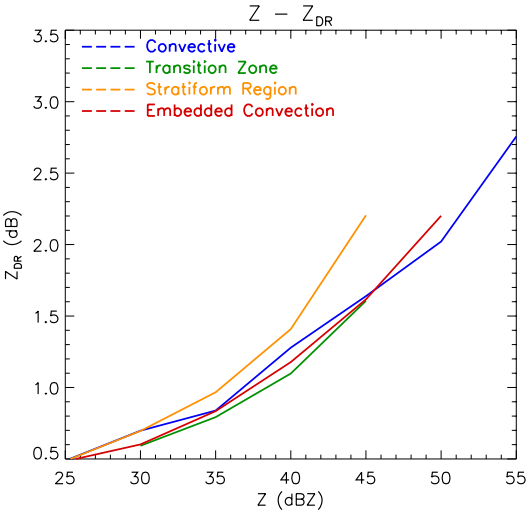

Fig. 7. Plot of Z-Z_{DR} for MCS precipitation regimes. Z_{DR} has been averaged over 5 dBZ reflectivity bins.

5. DSD dependence on freezing level height

Perhaps the most striking contrast found in this study is when DSDs are compared with respect to freezing level height. Fig. 8 presents a comparison of all data collected at freezing level heights between 1 – 2 km (blue), 2 – 3 km (green), 3 – 4 km (red), and 4 – 5 km (purple), while Fig. 9 depicts the same comparison when only stratiform regions are considered. Both figures illustrate the importance of environmental factors in the determination of dominant drop sizes in DSDs and, subsequently, polarimetric measurements at ground level. They also explain, in part, much of the seasonal variability depicted in Fig. 1. Fig. 8 clearly shows that, the higher the freezing level, the smaller the drops and corresponding Z_{DR}, at least for all Z > 30 dBZ. The results in Fig. 8, are particularly intriguing when analyzed in the context of the results presented in Fig. 9, which shows the same comparison, but for only stratiform precipitation. The data presented in Fig. 9 show that, for Z > 35 dBZ, the lower the freezing level, the higher the Z_{DR} for any given Z. For Z < 35 dBZ, however, the signature is just the opposite. As noted by discussion in section 2, high Z_{DR} measurements in the stratiform region can probably be attributed to a combination of processes that might lead to an abundance of large drops and a deficit of small drops. The large drops can result from the melting of large aggregates in the bright band region whereas the deficit at the small drop side of the spectrum might be attributed to evaporation of the very smallest drops in the unsaturated mesoscale downdraft. The profiles presented here suggest that when the freezing level is low, the relatively high Z_{DR} for Z > 35 dBZ might be attributable to the many large drops that make it to ground because they have less time to melt, whereas the lower Z_{DR} for Z < 35 dBZ might be attributable to an environment where less evaporation of small drops might be taking place.

6. DSD dependence on surface temperature

Another method of explaining potential seasonal variations in DSDs is to stratify the results according to surface temperatures. Fig. 10 presents a comparison of all data collected at surface temperatures between 0 – 5°C (blue), 5 – 10°C (green), 10 – 15°C (orange), 15 – 20°C (red), and 20 – 25°C (purple), while Fig. 11 depicts the same comparison when only stratiform regions are considered. From a quick inspection, it is obvious that surface temperature plays a much smaller role in determining observed DSDs than does freezing level height. In general, very few distinguishable trends can be seen when the data are compared with respect to surface temperature. In Fig. 10, there does

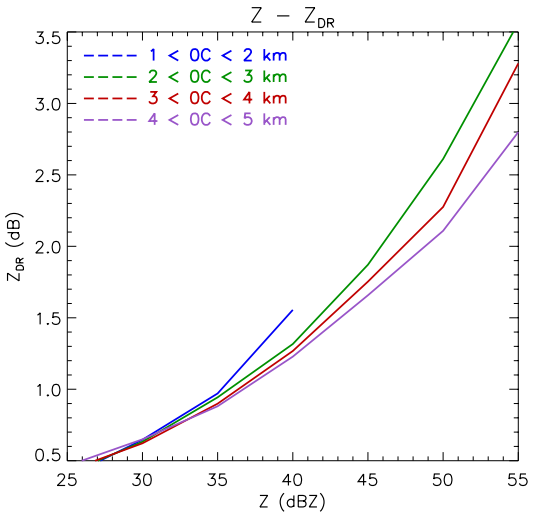

Fig. 8. Plot of Z-Z_{DR} by freezing level height for all data in the dataset. Z_{DR} has been averaged over 5 dBZ reflectivity bins.

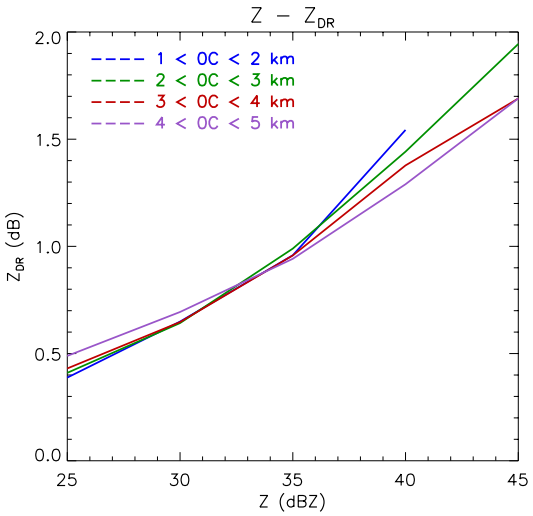

Fig. 9. Same as Fig. 8, except only for stratiform data points.

appear to be a slight preference for precipitation that occurs at warmer surface temperatures to have smaller drops and correspondingly smaller Z_{DR}s for any given Z. An examination of Fig. 11, however, suggests that there may be a slight crossover between 30 and 35 dBZ (similar to that seen in Figs. 8 and 9) where just the opposite is true. In any case, surface temperature does not appear to be a viable proxy for distinguishing between cold and warm season precipitation types for the purposes of rainfall estimation, at least not when it's utility is compared to that of freezing level height.

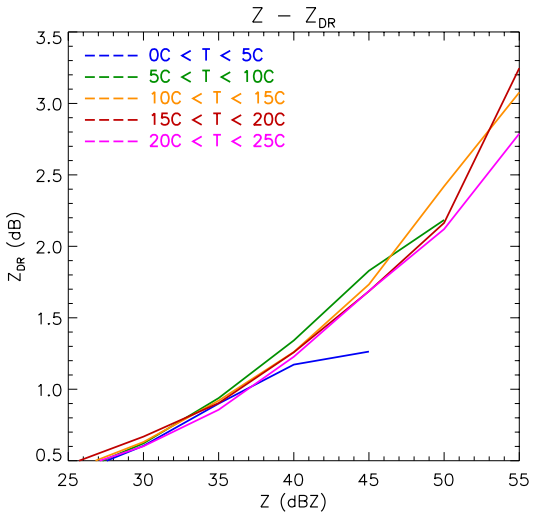

Fig. 10. Plot of Z-Z_{DR} by surface temperature for all data in the dataset. Z_{DR} has been averaged over 5 dBZ reflectivity bins.

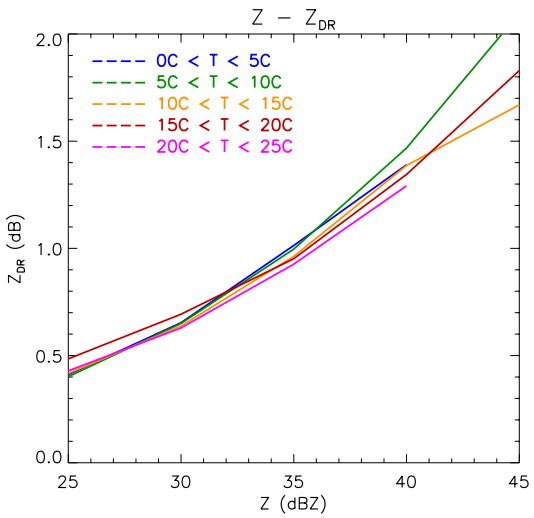

Fig. 11. Same as Fig. 10, except only for stratiform data points.

7. Big drops

Over the course of many years of data collection, we have found that large drops occur in a variety of precipitation types and environmental conditions. Of the 273 events that comprise this dataset, 182 events were found to contain drops at least 4 mm in size, 122 events with drops at least 5 mm in size, 75 events with drops at least 6 mm in size, and 36 events with drops at least 7 mm in size. As a proxy to investigate the frequency of DSDs with large drops in our studies, we have chosen a median volume diameter (D_0, computed in this study from the actual data rather than a functional fit) of 2.5 mm or greater to be representative of a large drop distribution. Of the 47,000 DSD in this study, we found that only 2% had a D_0 > 2.5 mm. More importantly, however, those 2% of the DSDs accounted for greater than 10% of the rainfall in our sample, with the frequency of occurrence weighted heavily towards the higher rain rates. When the frequency of DSDs with D_0 > 2.5 mm is broken down in more detail by eliminating all rain rates < 20 mm h^{-1} from our sample, we find that 20% of the DSDs that had rain rates > 20 mm h^{-1} had a D_0 > 2.5 mm. When analyzed by month, we find that the greatest frequency of DSDs with D_0 > 2.5 mm occurs during late spring, when strong convection that can often contain drops with small ice cores may be present.

8. Summary

The extreme natural variability seen in the DSDs by season, precipitation type, and environmental conditions such as freezing level height highlight the challenges of radar-based rainfall estimation techniques. On average, the largest Z_{DR} with respect to Z, indicative of DSDs with an abundance of large drops and/or a deficit of small drops, is most prevalent during the spring months. Sometimes tremendous variation is found when the DSDs are compared according to precipitation type. When MCS stratiform and SYNOP stratiform are compared, we find that MCS stratiform tends to have larger drops, or at least higher Z_{DR} with respect to Z, at all reflectivities, but particularly for the highest stratiform reflectivities of approximately 45 dBZ. We believe this is an indication of the strong influence of the convective line on the dynamics and precipitation structure of the MCS stratiform region. Likewise, quite distinct precipitation regimes can be seen in the DSD data when MCS convective line, transition zone, stratiform, and embedded convection region are compared.

Perhaps the most intriguing signature seen in this study is the strong dependence of the observed DSDs on the freezing level height, providing evidence of the strong relationship between observed DSDs and environmental factors. When all of the data with Z > 30 dBZ were considered, the lower the freezing level height, the higher the Z_{DR} with respect to Z. When stratiform only was considered, there was an interesting intersection of the profiles at approximately 35 dBZ. Above that reflectivity threshold, the stratiform profile followed that of that presented for the entire dataset. Below that reflectivity threshold, just the opposite was true. A much less strong dependence was found when DSDs were compared with surface temperature under which they were measured, suggesting that it is not appropriate to use surface

temperature alone as a proxy for determining warm and cold precipitation regimes.

Statistics derived from this dataset indicate that large drops are fairly common in precipitation systems over the southern Great Plains. While sometimes accounting for only a small fraction of the total precipitation, they were found to account for a much larger portion of the total rainfall. This was especially true for rain rates > 20 mm h^{-1}.

Acknowledgements

This conference paper was prepared by Terry Schuur with funding provided by NOAA/Office of Oceanic and Atmospheric Research under NOAA-University of Oklahoma Cooperative Agreement #NA17RJ1227, U.S. Department of Commerce. The statements, findings, conclusions, and recommendations are those of the authors and do not necessarily reflect the views of NOAA or the U.S. Department of Commerce.

The authors would like to acknowledge funding support for this work from the National Weather Service, the Federal Aviation Administration, and the Air Force Weather Agency through the NEXRAD Product Improvement Program.

The authors would also like to thank Oklahoma Climate Survey for supplying the Oklahoma mesonet data that was used in this study.

References

Brandes, E. A., G. Zhang, and J. Vivekanandan, 2002: Experiments in rainfall estimation with a polarimetric radar in a subtropical environment. *J. Appl. Meteor.*, **41**, 674-685.

Brandes, E. A., G. Zhang, and J. Vivekanandan, 2005: Corrigendum. *J. Appl. Meteor.* **44**, 186–186.

Brown, J. M., 1979: Mesoscale unsaturated downdrafts driven by rainfall evaporation: A numerical study. *J. Atmos. Sci.*, 36, 313-338.

Ryzhkov, A. V., S. E. Giangrande, and T. J. Schuur, 2005: Rainfall estimation with a polarimetric prototype of WSR-88D. *J. Appl. Meteor.*, **44**, 502-515.

Schuur, T. J., A. V. Ryzhkov, D. S. Zrnić, and M. Schönhuber, 2001: Drop size distributions measured by a 2D video disdrometer: Comparison with dual-polarization radar data. *J. Appl. Meteor.*, 40, 1019-1034.